Original Article
The distribution of Mn^{2+} in rabbit eyes after topical administration for manganese-enhanced MRI

Shenzhi Liang[1], Miao Liang[2], Yu Zhu[1], Jingliang Cheng[3], Zitao Yang[3]

[1]Department of Ophthalmology, First Affiliated Hospital of Zhengzhou University, Zhengzhou, China; [2]School of Food and Bioengineering, Zhengzhou University of Light Industry, Zhengzhou, China; [3]Department of MRI, First Affiliated Hospital of Zhengzhou University, Zhengzhou, China

Abstract: Purpose: To analyze the distribution of Mn^{2+} in rabbit eyes after topical administration of $Mncl_2$ for manganese-enhanced MRI. Methods: Forty-eight Chinese white rabbits were divided into three groups. In group 1 (n = 4), the baseline concentration of Mn^{2+} in aqueous, vitreous and serum samples were analyzed. In group 2 and 3, the rabbits received one topical instillation (20 μL) of $MnCl_2$ (1 mol•L^{-1}). In group 2 (n = 40), aqueous, vitreous and serum samples were collected and analyzed at predetermined time points (0.5, 1, 2, 4, 6, 12, 24, 48, 72 and 168 hours postdose). Assays were performed using inductively coupled plasma-mass spectrometer (ICP-MS). In group 3 (n = 4), after topical administration of $MnCl_2$, dynamic manganese-enhanced MRI (MEMRI) was performed at predetermined time points. The signal-to-noise ratio (SNR) was calculated to evaluate the enhancements of eyes. Results: After topical administration, the maximum concentrations of Mn^{2+} in the aqueous and vitreous samples were 11.1641 ± 0.7202 (2 hours) and 1.5622 ± 0.1567 (12 hours). In group 3, the maximum enhancement of aqueous humor (SNR = 108.81 ± 10.65) appeared at 2 hours postdose, whereas, no significant changes were detected in vitreous. Conclusion: Mn^{2+} could distribute into aqueous humor rapidly after topical administration of $MnCl_2$, whereas, the concentration of Mn^{2+} in vitreous body fluctuated in a narrow range over the course. The uptake of Mn^{2+} in retina may involve several different pathways.

Keywords: Drug distribution, manganese, topical administration, MEMRI, ICP-MS

Introduction

Manganese (Mn^{2+}) enters cells through voltage gated calcium channels and then moves along axons via axonal transport [1, 2]. Given the paramagnetic nature of Mn^{2+}, its uptake and transport in the nervous system is detectable by MRI with T1-weighted imaging (T1WI). Manganese-enhanced MRI (MEMRI) has recently been used as a biomarker and tracer to investigate optic nerve axonal integrity [3-8], retinal projections to the superior colliculus [9], layer-specific calcium-dependent retinal fMRI activation [10, 11], cortical response to stimulation or postnatal development and plasticity of retinal and callosal projections [12, 13].

When MEMRI is used to investigate the visual system, an intravitreal injection is the common means of delivery of the Mn^{2+} solution into the ocular space [3, 14-16]. However, direct injection of drugs into the vitreous body is stressful

for patients and could potentially produce severe adverse events, such as endophthalmitis, retinal detachment, uveitis, ocular hypertension, cataract, intraocular hemorrhage, and hypotony [17]. In an attempt to remedy the invasive intravitreal injection of $MnCl_2$, Sun SW et al. proposed to deliver Mn^{2+} through topical loading [18, 19]. In their study, they considered that the uptake of Mn^{2+} may do not involve the vitreous body. But the definite conclusion can not be established from the observed lack of vitreous enhancement in previous studies.

To investigate the penetration and distribution of Mn^{2+} after topical administration of $Mncl_2$, we measured the concentration of Mn^{2+} in aqueous humor and vitreous body in rabbits. And, MEMRI was performed at same time, to analyze the relation of the enhancement of eyes and Mn^{2+} concentration in aqueous humor and vitreous body.

Table 1. The time course of Mn^{2+} Concentrations in aqueous humor, vitreous body and serum after topical administration of Mncl$_2$ (1 mol•L^{-1})

Time (h)	Aqueous humor (mg•L^{-1})	Vitreous body (mg•L^{-1})	Serum (mg•L^{-1})
Control	0.2136 ± 0.0183	0.2234 ± 0.0154	0.2379 ± 0.0093
0.5	5.3062 ± 0.3011☆	0.2713 ± 0.0154☆	0.2435 ± 0.0164
1	7.9690 ± 0.4721☆	0.3011 ± 0.0148☆	0.2431 ± 0.0161
2	11.1641 ± 0.7202☆	0.5012 ± 0.0125☆	0.2309 ± 0.0137
4	5.4838 ± 0.6073☆	1.2195 ± 0.0977☆	0.2341 ± 0.0124
6	2.2523 ± 0.1921☆	1.2786 ± 0.1504☆	0.2401 ± 0.0152
12	1.9814 ± 0.2019☆	1.5622 ± 0.1567☆	0.2236 ± 0.0141
24	1.6626 ± 0.2833☆	1.0453 ± 0.1336☆	0.2283 ± 0.0129
48	0.8640 ± 0.1750☆	0.7322 ± 0.1480☆	0.2309 ± 0.0168
72	0.4936 ± 0.1702☆	0.3612 ± 0.0755☆	0.2256 ± 0.0114
168	0.2301 ± 0.0209	0.2435 ± 0.0206	0.2321 ± 0.0132

☆$P < 0.01$, compared with control group.
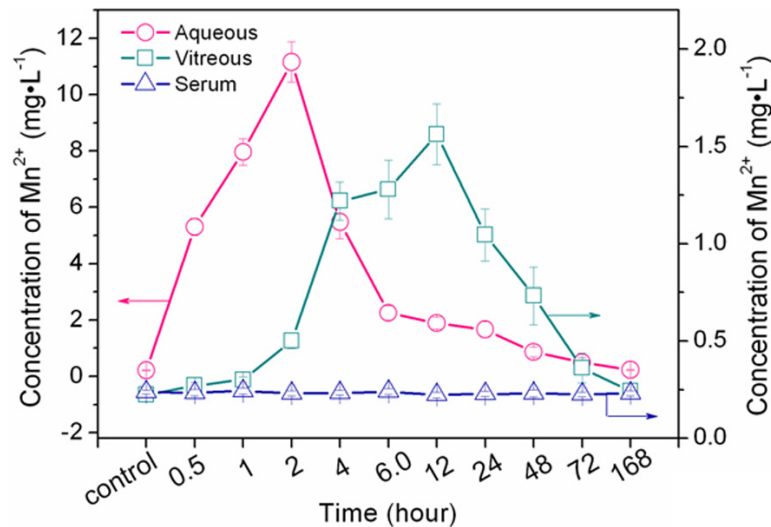
Figure 1. Mn^{2+} concentrations versus time profiles in aqueous humor, vitreous body and serum after topical administration of Mncl$_2$ (20 μL, 1 mol•L^{-1}). The maximum concentrations of Mn^{2+} in aqueous humor and vitreous body were 11.1641 ± 0.7202 mg•L^{-1} (2 hours) and 1.5622 ± 0.1567 mg•L^{-1}. The concentration of Mn^{2+} decreased rapidly. The concentration in vitreous body fluctuated in a narrow range, and no obvious changes were detected in serum.

Materials and methods

Animals and groups

Forty-eight Chinese white rabbits were divided into three groups, 1) control group (n = 4), to analyze the baseline concentration of Mn^{2+} in aqueous humor, vitreous body and serum. 2) concentration test group, in which the concentrations of Mn^{2+} in aqueous humor, vitreous body and serum were analyzed at predeter-

mined time points after topical administration of MnCl$_2$. 3) MEMRI group (n = 4), to visualize the enhancement images after administration of MnCl$_2$.

The rabbits (supplied by Zhengzhou University Experimental Animal Center) of mixed gender and an average age of 15 weeks were reared in room with standard chow and water supply. Animals were treated in accordance with the guidelines of the Association for Research in Vision and Ophthalmology and protocols approved by the Zhengzhou University Animal Ethical Committee for animal research.

MnCl$_2$ administration

For topical administration of MnCl$_2$, 1.0 mol·L^{-1} MnCl$_2$ in distilled and deionized water was freshly prepared (PH = 6.5). The rabbits were anesthetized with xylazine (5 mg•kg^{-1}) and ketamine (35 mg•kg^{-1}). Utilizing a micropipette, the left eye of rabbits in group 2 (n = 40) and MEMRI group (n = 4) received one topical instillation (20 μl) of MnCl$_2$.

Samples collection

In group 2 (n = 40), at predetermined time points (0.5, 1, 2, 4, 6, 12, 24, 48, 72 and 168 hours postdose), 4 rabbits were first anesthetized with xylazine (5 mg•kg^{-1}) and ketamine (35 mg•kg^{-1}). A sample of arterial blood was drawn from the central artery of the ears just before the euthanasia. Rabbits were then sacrificed with pentobarbital overdose (1.2 ml•kg^{-1}). The left eyes were enucleated and then rinsed with an isotonic saline solution. The aqueous humor (0.15 ml) was removed from the eye using a 1-ml syringe attached to a 27-gauge needle. Vitreous body (0.15 ml) was
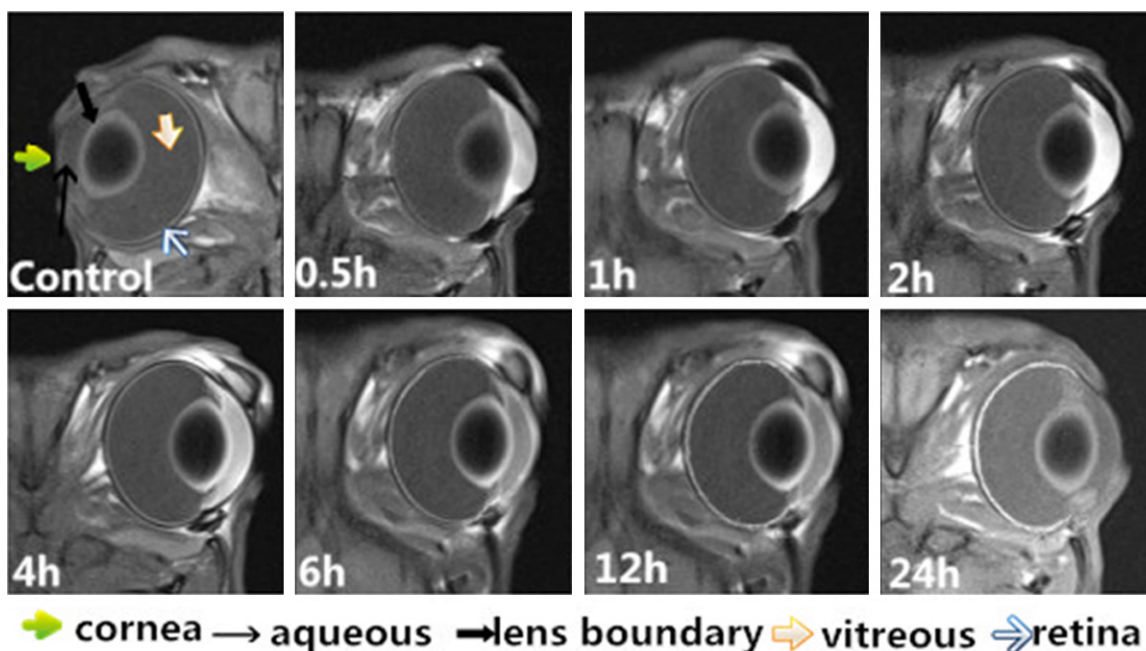
Figure 2. Dynamic images of the rabbit eyes (T1WI) after topical administration of Mncl$_2$ (1 mol•L^{-1}) at predetermined time points (0.5, 1, 2, 4, 6, 12 and 24 hours postdose). The enhancement of cornea and aqueous humor began at 0.5 hour, the maximum enhancement appeared at 2 hours, and then gradually decreased. There were no obvious enhancement of vitreous body during the follow up.

aspired with a 15-gauge needle mounted on a 5-ml syringe. Serum was obtained by allowing the blood sample to clot at room temperature for 1 hour followed by centrifugation. All samples were diluted to 15 ml with distilled and deionized water. The 4 rabbits in group 3 were sacrificed and samples were obtained as mentioned above.

Mass spectrometry analysis of Mn^{2+}

The concentrations of Mn^{2+} were analyzed on a PE/SCIEX Elan 6100 inductively coupled plasma-mass spectrometer (ICP-MS, Perkin Elmer Life & Analytical Sciences, Shelton, Connecticut, USA). All samples were vortexed and aspirated into a pneumatic nebulizer. The resulting aerosol was directed to the hot plasma discharge by a flow of argon. Instrumentation response was defined by the linear relationship of analyte concentration vs ion counts. Analyte concentrations were derived by reading the ion count ratio for each mass of interest.

Memri

In group 3 (n = 4), T1WI was repeated at predetermined time points (0.5, 1, 2, 4, 6, 12, 24, 48,

72 and 168 hours postdose). MRI was performed using a clinical 3.0 Tesla scanner (Siemens, Germany), with a 3-inch surface coil as a receiver. The employed sequence acquired data with the following parameters: voxel size, 0.2 × 0.2 × 2 mm, matrix 448 × 314, echo time TE = 16 ms, repetition time TR = 600 ms, band width = 199 Hz/px, a total TA (acquisition time) of approximately 8 minutes was achieved.

Manually drawn regions of interest (ROIs) were placed in oblique 2D slices. The mean signal intensities of aqueous humor and vitreous body were measured. The signal-to-noise ratio (SNR) was calculated with the following formula: SNR = S/SDair. Where S represents the signal intensity in the ROI of the Mn^{2+} enhanced area, and SDair is the mean value of the SD in three ROIs in air.

Statistical analysis

Data were given as mean ± standard error and analyzed by SPSS15.0. The concentration of Mn^{2+} and SNR at predetermined time points were compared to the baseline concentration and SNR of rabbit eyes in control group, using independent sample t-test. $P < 0.01$ was considered statistically significant.

Table 2. The SNR of eyes at predetermined time points after topical administration of Mncl$_2$ (1 mol•L^{-1})

Time (h)	Aqueous humor	Vitreous body
Control	27.12 ± 1.88	28.45 ± 1.81
0.5	99.77 ± 2.26※	29.26 ± 2.24
1	105.21 ± 3.92※	25.33 ± 1.05
2	108.81 ± 10.65※	29.03 ± 1.97
4	85.66 ± 5.08※	30.23 ± 1.87
6	75.25 ± 6.30※	30.44 ± 1.79
12	62.61 ± 5.41※	31.13 ± 2.05
24	37.54 ± 3.95※	29.95 ± 2.38
48	31.02 ± 5.09	32.36 ± 2.33
72	28.08 ± 5.76	28.38 ± 2.64
168	28.74 ± 4.03	30.55 ± 1.83

※$P < 0.01$, compared with control group, (SNR, Signal-to-Noise ratio).

Results

Measurement of Mn^{2+} concentration

The concentrations of Mn^{2+} versus time profiles in aqueous humor, vitreous body and serum after topical administration are shown in **Table 1**. The concentration of Mn^{2+} in aqueous humor increased rapidly 0.5 hours after topical administration, and the maximum was measured at 2 hours (11.1641 mg•L^{-1}). Then the concentration decayed rapidly, and the concentration decreased to 2.2523 mg•L^{-1} at 6 hours. The concentrations of Mn^{2+} in aqueous humor at predetermined time points (0.5, 1, 2, 4, 6, 12, 24, 48, and 72 hours postdose) were significantly different from the control group. ($P < 0.01$) In vitreous body, the concentration of Mn^{2+} increased slowly 0.5 hours postdose, the maximum concentration was measured at 12 hours (1.5622 mg•L^{-1}). The concentration of Mn^{2+} in aqueous humor and vitreous body decreased to the baseline at 168 hours. Whereas, no obvious changes of Mn^{2+} concentration were detected in serum at all times throughout the study (**Figure 1**).

MEMRI of eyes

In group 3, we obtained the repeated T1WIs of eyes, at predetermined time points (0.5, 1, 2, 4, 6, 12, 24, 48, 72 and 168 hours postdose) after MnCl$_2$ (20 μL, 1 mol•L^{-1}) loading. Data collected from right eyes without Mn^{2+} treatments were added as a control. The aqueous humor showed initial significant enhancement 0.5 hour after MnCl$_2$ loading, and reached the peak at 2 hours postdose. The enhancement of aqueous humor began to decrease after 2 hours postdose. Whereas, there were no obvious enhancement of vitreous body during the follow up (**Figure 2**).

The SNR of different tissue versus time profiles are shown in **Table 2**. The SNRs of aqueous humor at 0.5, 1, 2, 4, 6, 12 and 24 hours postdose were significantly different from the control eyes. ($P < 0.01$). Whereas, the vitreous body did not show significant changes in the entire temporal evaluation.

Discussion

There is increasing interest in developing MEMRI as a technique for functional and molecular imaging of biological processes, and Mn^{2+} is now a well-established contrast agent in this technique [7-9]. Recently, Sun SW et al have demonstrated the feasibility of using topical administration of Mn^{2+} for MEMRI [18]. The penetration and distribution of Mn^{2+} is a complicated process, for further study of topical administration of Mn^{2+} for MEMRI, we evaluated the concentration of Mn^{2+} in aqueous humor and vitreous body using ICP-MS, and analyzed the relation of Mn^{2+} concentration and enhancement of eyes in rabbits.

ICP-MS is a specific detector for metals at extremely low level. It plays an increasingly major role in trace elements analysis in different aspects [20-23]. In the study, the Mn^{2+} concentration in aqueous humor began to increase 0.5 hour after topical administration of Mncl$_2$. The concentration increased rapidly with an initial burst effect at the early stage, and then reached maximum concentration at 2 hours. MEMRI showed the enhancement of aqueous humor synchronized with the fluctuation of the Mn^{2+} concentration in aqueous humor. The maximum SNR of the aqueous humor emerged at 2 hours (108.81 ± 10.65). The releasing model of Mn^{2+} was consistent with many topical administration drugs [24-27].

In previous study, MEMRI showed there were no detectable changes of signal intensity in vitreous body after topical administration of Mncl$_2$. SUN SW et al concluded that the uptake

of Mn^{2+} might do not involve the vitreous body [18]. But they did not measure the Mn^{2+} concentration in vitreous body. In the study, although the vitreous body did not show obvious enhancement of MEMRI, the concentration of Mn^{2+} fluctuated during the follow up times. We found that the Mn^{2+} concentration in vitreous body began to increase slowly 0.5 hour after administration of Mncl$_2$, and the maximum concentration was measured on 12 hours (1.5622 mg•L^{-1}).

In the study, the Mn^{2+} concentration was very low in vitreous body. These findings suggested that the uptake of Mn^{2+} in retina may do not involve the vitreous body or the Mn^{2+} enters the retina via other different routes. The specific transport pathways across eye tissues can alter the passive permeation, such as ion channels or membrane transporters. The previous studies confirmed that the enhancement depended on the health retina ganglia cells (RGCs), the loss of RGCs can minimize the amount of Mn^{2+} that enters the cells [18, 28-30]. As a calcium analog, the calcium channels in cells may affect the absorption of Mn^{2+} in retina, and cause the significant enhancement of retina.

The presented study evaluated the concentration of Mn^{2+} in aqueous humor and vitreous body after topical administration of Mncl$_2$, and analyze the relationship of the enhancement of MEMRI and Mn^{2+} concentration of eyes in rabbits. Whereas, our study was compromised by several limitations. In the study, we just investigated the concentration of Mn^{2+} in aqueous humor and vitreous body, but the concentrations of Mn^{2+} in cornea, lens boundary, retina and optic nerve were not included.

In conclusion, after topical administration of Mncl$_2$, Mn^{2+} could distribute into aqueous humor rapidly, whereas, the Mn^{2+} concentration in vitreous body fluctuated in a narrow range over the course. There were no significant enhancement in vitreous body. Maybe the uptake of Mn^{2+} in retina did not involve vitreous body, or it involved several different pathways.

Acknowledgements

Disclosure of conflict of interest

None.

Address correspondence to: Dr. Yu Zhu, Department of Ophthalmology, First Affiliated Hospital of Zhengzhou University, No. 1 East of Road Jianshe, Zhengzhou 450052, Henan Province, China. Tel: +86 13673666718; Fax: +8637166862921; E-mail: zhuzzdx@163.com

References

[1] Pautler RG. In vivo, trans-synaptic tract-tracing utilizing manganese-enhanced magnetic resonance imaging (MEMRI). NMR Biomed 2004; 17: 595-601.

[2] Sloot WN, Gramsbergen JB. Axonal transport of manganese and its relevance to selective neurotoxicity in the rat basal ganglia. Brain Res 1994; 657: 124-132.

[3] Boretius S, Gadjanski I, Demmer I, Bahr M, Diem R, Michaelis T, Frahm J. MRI of optic neuritis in a rat model. Neuroimage 2008; 41: 323-334.

[4] Gadjanski I, Boretius S, Williams SK, Lingor P, Knoferle J, Sattler MB, Fairless R, Hochmeister S, Suhs KW, Michaelis T, Frahm J, Storch MK, Bahr M, Diem R. Role of n-type voltage-dependent calcium channels in autoimmune optic neuritis. Ann Neurol 2009; 66: 81-93.

[5] Thuen M, Olsen O, Berry M, Pedersen TB, Kristoffersen A, Haraldseth O, Sandvig A, Brekken C. Combination of Mn (2+)-enhanced and diffusion tensor MR imaging gives complementary information about injury and regeneration in the adult rat optic nerve. J Magn Reson Imaging 2009; 29: 39-51.

[6] Berkowitz BA, Bissg D, Dutczak O, Corbett S, North R, Roberts R. MRI biomarkers for evaluation of treatment efficacy in preclinical diabetic retinopathy. Expert Opin Med Diagn 2013; 7: 393-403.

[7] Nair G, Pardue MT, Kim M, Duong TQ. Manganese-Enhanced MRI Reveals Multiple Cellular and Vascular Layers in Normal and Degenerated Retinas. J Magn Reson Imaging 2011; 34: 1422-1429.

[8] Chan KC, Fu QL, Hui ES, So KF, Wu EX. Evaluation of the retina and optic nerve in a rat model of chronic glaucoma using in vivo manganese-enhanced magnetic resonance imaging. Neuroimage 2008; 40: 1166-1174.

[9] Chan KC, Li J, Kau P, Zhou IY, Cheung MM, Lau C, Yang J, So KF, Wu EX. In vivo retinotopic mapping of superior colliculus using manganese-enhanced magnetic resonance imaging. Neuroimage 2011; 54: 389-395.

[10] De La Garza BH, Li G, Shih YY, Duong TQ. Layer-specific manganese enhanced MRI of the retina in light and dark adaptation. Invest Ophthalmol Vis Sci 2012; 53: 4352-4358.

[11] Berkowitz BA, Roberts R, Goebel DJ, Luan H. Noninvasive and simultaneous imaging of layer-specific retinal functional adaptation by manganese-enhanced MRI. Invest Ophthalmol Vis Sci 2006; 47: 2668-2674.

[12] Bissig D, Berkowitz BA. Manganese-enhanced MRI of layer-specific activity in the visual cortex from awake and free-moving rats. Neuroimage 2009; 44: 627-635.

[13] Chan KC, Cheng JS, Fan S, Zhou IY, Yang J, Wu EX. In vivo evaluation of retinal and callosal projections in early postnatal development and plasticity using manganese-enhanced MRI and diffusion tensor imaging. Neuroimage 2012; 59: 2274-2283.

[14] Lindsey JD, Scadeng M, Dubowitz DJ, Crowston JG, Weinreb RN. Magnetic resonance imaging of the visual system in vivo: transsynaptic illumination of V1 and V2 visual cortex. Neuroimage 2007; 34: 1619-1626.

[15] Olsen O, Thuen M, Berry M, Kovalev V, Petrou M, Goa PE, Sandvig A, Haraldseth O, Brekken C. Axon tracing in the adult rat optic nerve and tract after intravitreal injection of MnDPDP using a semiautomatic segmentation technique. J Magn Reson Imaging 2008; 27: 34-42.

[16] Berkowitz BA, Roberts R, Goebel DJ, Luan H. Noninvasive and simultaneous imaging of layer-specific retinal functional adaptation by manganese-enhanced MRI. Invest Ophthalmol Vis Sci 2006; 47: 2668-2674.

[17] Jager RD, Aiello LP, Patel SC, Cunningham ET Jr. Risks of intravitreous injection: a comprehensive review. Retina 2004; 24: 676-698.

[18] Sun SW, Campbell B, Lunderville C, Won E, Liang HF. Noninvasive topical loading for manganese-enhanced MRI of the mouse visual system. Invest Ophthalmol Vis Sci 2011; 52: 3914-3920.

[19] Sun SW, Thiel T, Liang HF. Impact of Repeated Topical-Loaded Manganese-Enhanced MRI on the Mouse Visual System. Invest Ophthalmol Vis Sci 2012; 53: 4699-4709.

[20] Konz I, Fernandez B, Fernandez ML, Pereiro R, Gonzalez-Iglesias H, Coca-Prados M, Sanz-Medel A. Quantitative bioimaging of trace elements in the human lens by LA-ICP-MS. Anal Bioanal Chem 2014; 406: 2343-2348.

[21] Krachler M. Environmental applications of single collector high resolution ICP-MS. J Environ Monit 2007; 9: 790-804.

[22] Balcaen L, Bolea-Fernandez E, Resano M, Vanhaecke F. Accurate determination of ultratrace levels of Ti in blood serum using ICP-MS/MS. Analytica Chimica Acta 2014; 809: 1-8.

[23] Erie JC, Butz JA, Good JA, Erie EA, Burritt MF, Cameron JD. Heavy metal concentrations in human eyes. Am J Ophthalmol 2005; 139: 888-893.

[24] Ozturk F, Kortunay S, Kurt E, Ilker SS, Basci NE, Bozkurt A. Penetration of topical and oral ciprofloxacin into the aqueous and vitreous humor in inflamed eyes. Retina 1999; 19: 218-222.

[25] Goldblum D, Fausch K, Frueh BE, Theurillat R, Thormann W, Zimmerli S. Ocular penetration of caspofungin in a rabbit uveitis model. Graefe's Arch Clin Exp Ophthalmol 2007; 245: 825-833.

[26] Sakarya R, Sakarya Y, Ozcimen M, Kesli R, Alpfidan I, Kara S. Ocular penetration of topically applied 1% daptomycin in a rabbit model. J Ocul Pharmacol Ther 2013; 29: 75-78.

[27] Zhang JJ, Wang LY, Zhou J, Zhang L, Xia HY, Zhou TY. Ocular penetration and pharmacokinetics of topical clarithromycin eye drops to rabbits. J Ocul Pharmacol Ther 2014; 30: 42-48.

[28] Zheng L, Gong BD, Hatala DA, Kern TS. Retinal ischemia and reperfusion causes capillary degeneration: similarities to diabetes. Invest Ophthalmol Vis Sci 2007; 48: 361-367.

[29] Song SK, Sun SW, Ju WK, Lin SJ, Cross AH, Neufeld AH. Diffusion tensor imaging detects and differentiates axon and myelin degeneration in mouse optic nerve after retinal ischemia. Neuroimage 2003; 20: 1714-1722.

[30] Feng Y, Luo LS, Ma ZZ, Sun XD, Hu YT. In vivo detection of severity of optic nerve crush using manganese-enhanced magnetic resonance imaging in rats. Chin Med J (Engl) 2014; 127: 522-527.